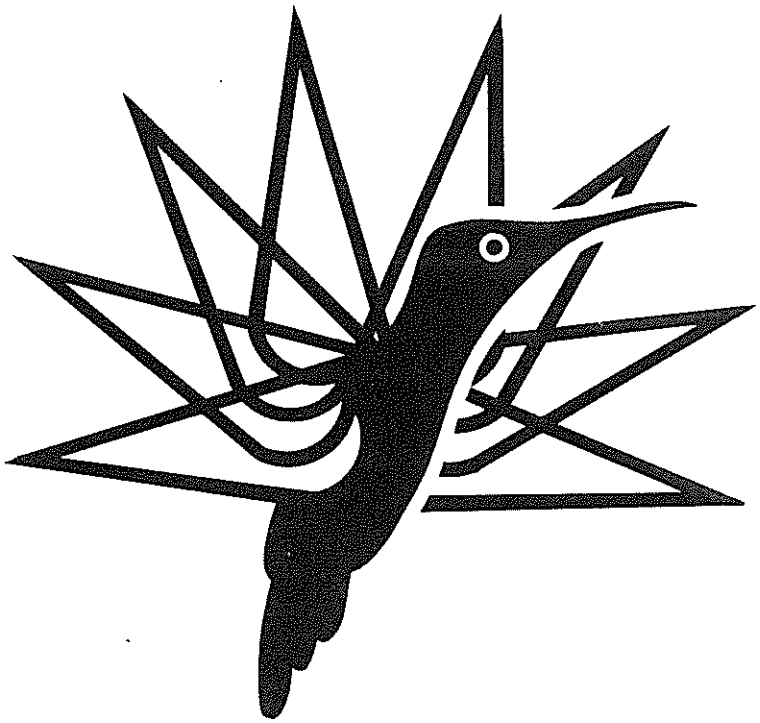

MODEL TESTS FOR AN ACTIVE ROTOR ISOLATION SYSTEM

by

R. Mehlhose, M. Obermayer

Messerschmitt-Bölkow-Blohm GmbH
Munich, Germany

M. Degener

Deutsche Forschungs- und Versuchsanstalt für Luft- und Raumfahrt e.V., Institut für Aeroelastik
Göttingen, Germany

FIFTH EUROPEAN ROTORCRAFT AND POWERED LIFT AIRCRAFT FORUM
SEPTEMBER 4 – 7TH 1979 - AMSTERDAM, THE NETHERLANDS

MODEL TESTS FOR AN ACTIVE ROTOR ISOLATION SYSTEM *)

R. Mehlhose, M. Obermayer

Messerschmitt-Bölkow-Blohm GmbH
Munich, Germany

M. Degener

Deutsche Forschungs- und Versuchsanstalt für Luft- und Raumfahrt e.V., Institut für Aeroelastik
Göttingen, Germany

*) Work sponsored by the German Ministry of Research and Technology (BMFT)

Abstract

Analytical studies, started in 1975, indicate that an active rotor isolation system with disturbance rejection control is a powerful means to reduce rotor-induced helicopter vibrations.

This paper presents experimental results of a single-axis, full-scale laboratory research model which was defined for investigations into an active isolation concept.

The tests were conducted on an electrohydraulic actuator with time continuous pressure feedback and digital disturbance rejection controllers. Special attention was given to the development of efficient control algorithms with differing sample-and-hold devices. The investigations show that a special kind of data hold is necessary.

Measurements in the time and frequency domains are compared with theoretical calculations. Good correlation is demonstrated between theory and experiment.

The tests show that extremely high vibration reduction can be achieved by an active isolation system consistent with modern technology.

Notation

A	Actuator area
a_i, b_i, c_i, d_i, w_i	Reduced system matrix coefficients
A_i, B_i, C_i, W_i	Complete system matrix coefficients
d, k	Damper, spring
D	Discrete-time transfer function
F	Force
G	Continuous-time transfer function
K, k	Coefficients
m	Mass
n_o	Trim integrator variable
n_1, n_2	Notch variables

Δp	Differential pressure
q	Hydraulic flow
s	Laplace variable
t	Time variable
T	Sample-and-hold time; time constant
z	Vertical displacement
ε	Servovalve piston displacement
ζ	Damping ratio
$\Psi = \Omega t$	Rotor azimuth angle
Ω	Rotor frequency
ω	Frequency

Subscripts

A	Actuator
F	Fuselage
h	Hold
I	Isolator
R	Rotor/transmission unit
SV	Servovalve
Δ	Support spring

Superscripts

$(\dot{}) = \frac{d}{dt}$	Time - differentiation
$(\,)' = \frac{d}{d\Psi}$	Azimuth angle - differentiation
$(\bar{})$	Normalized value

1. Introduction

During the last years nodal isolation systems for helicopters have been developed by several aircraft companies, but apart from one active system of the late 1960's all other systems have used passive isolation devices based on some kind of antiresonant vibration isolation. The reasons for developing a new active nodal isolation system resulted from the progress of technology in servo hydraulics and digital data processing, and of modern control theory for multivariable feedback design. Some further information about the advantages and problems of active rotor isolation is given in a paper to the Third European Rotorcraft and Powered Lift Aircraft Forum (Ref. 1, see also Ref. 2).

The model tests for this active rotor isolation system are an important part of the development of an active multi-axis, multi-fre-

quency nodal isolation system which can be applied to all helicopters. This isolation system, designated ASIS (Aktives Schwingungs-Isolations-System, i.e. active vibration isolation system) has been designed during the last four years by Messerschmitt-Bölkow-Blohm under sponsorship of the German Ministry of Research and Technology (BMFT) and in co-operation with two institutes of Deutsche Forschungs- und Versuchsanstalt für Luft- und Raumfahrt (DFVLR). To illustrate this system, Figure 1 shows a concept for development of the multi-axis isolation system applied to a light helicopter (e.g. BO 105 helicopter).

Following on from theoretical studies experimental investigations have been carried out with an electrohydraulic actuator coupled with a disturbance rejection digital controller. Tests took place at the DFVLR-Institut für Aeroelastik on a full-scale but single-axis laboratory research model which is able to simulate the major vibration behaviour of the BO 105 helicopter in the vertical axis. They have demonstrated that it is possible to realize this ambitious isolation concept by means of modern technology.

The purpose of this paper is to discuss the theoretical and experimental results, the efficiency of the selected vibration control concept, and to point out the possibilities that are offered to vibration control by active disturbance rejection.

2. Design Approach to an Active Vibration Control Concept

The selected rotor isolation system shown in Figure 1 isolates the rotor/transmission unit from the fuselage by special force isolator units. This concept which operates on resultant forces at the transmission feet is adaptable to all types of helicopters. Moreover the application of special isolator units permits a multi-axis, multi-frequency vibration isolation.

A rotor/transmission isolation system has to perform two tasks:

- The reduction of unmeasurable rotor disturbances by means of inertia forces and moments of the oscillating gearbox, while at the same time transferring static or quasistatic loads.
- The limitation of gearbox motions in manoeuvre flight owing to interfacing systems such as engines and controls.

These two tasks can be accomplished optimally by an active isolation system with appropriate disturbance rejection controllers:

- Airframe vibration control by notch isolator feedback of the transmitted isolator forces.
- Gearbox displacement control by integral feedback.

The isolator units shown in Figure 1 are composed of electrohydraulic actuators and parallel springs for support of the fuselage and as fail safe devices. Further information can be drawn from Reference 1 through 3.

3. Development of the Laboratory Research Model

3.1 Design

The laboratory research model of Figure 2 was developed in order to test the main components of the active rotor isolation system, in particular the electrohydraulic actuator and various digital control concepts. This model must accomplish two essential requirements:

- It had to be able to simulate the principal vibration properties of the flying helicopter in the vertical axis, in particular the first and second blade passage harmonics (4Ω = 28 Hz and 8Ω = 56 Hz).
- The servo controlled actuator had to be a full-scale model of those provided for the helicopter. For test reasons airworthiness was not demanded.

These requirements led to the following design concept of the laboratory research model (see Figure 3 and 4):

- Since, for simplicity, only one actuator is used instead of three for the vertical axis of the helicopter, the mass values were scaled by 1 : 3. This finally results in:

Fuselage and actuator mass	650	kg
Rotor/transmission mass	135	kg
Σ	685	kg

- The helicopter is simulated by two symmetric bodies, of which the inner one represents the fuselage and the outer one the rotor/transmission system. For the first tests the fuselage mass was designed as a rigid body which can be interchanged later by a flexible beam. The transmission mass is a rigid framework.
- The two bodies are connected by the force isolator consisting of the servoactuator and two parallel springs.
- Hydraulic power is supplied by a pressure-controlled pump.
- Rotor disturbances are simulated by an electrodynamic shaker.
- The sensors needed for control are a displacement transducer (piston displacement), a differential pressure transducer and an accelerometer (for the rigid fuselage mass the acceleration signal is equivalent to the transmitted isolator force).
- A minicomputer system (PDP11-40) is used as a digital disturbance rejection controller.
- An analogue controller is provided for pressure control of the actuator.
- In order to ensure only small deviations from the free-free flight vibration state, the rotor/transmission mass is suspended on a very soft air-spring.
- For preventing displacements of the two bodies in the horizontal axis, they are guided by auxiliary springs (plate springs) with low system frequencies in the vertical and relatively high frequencies in the horizontal axis.

The photographs of Figure 3 and 4 give further information about the test rig and the test model.

3.2 Measuring Equipment (see Figure 2)

Time-Domain Measurements - All signals were adapted and amplified by signal processing devices. In addition to the measured variables, piston velocity ($\Delta\dot{z}$) and acceleration ($\Delta\ddot{z}$) were generated by an electronic differentiator circuit. All time-dependent signals were recorded on-line on oscilloscopes, a magnetic tape recorder with 14 channels and an x-t-recorder with 8 channels. For very low-frequent measurements - for instance hysteresis curves - an x-y-recorder was used, too. Figure 5 shows a part of the measuring equipment.

Frequency-Domain Measurements - To record frequency response curves, i.e. magnitude and phase angle plots, all signals were resolved into their real and imaginary parts by vector component meters. Special process computers and programmes were used for generating Bode plots and amplitude spectra. More information about measuring equipment and sensors can be drawn from Reference 4.

3.3 Actuator and Servovalve

In order to realize active nodal isolation, all system components - actuator, servovalve, sensors and control - have to satisfy stringent requirements, but surely the servoactuator is the most critical component. Thus, its design was one of the most important and interesting items. A photograph of the actuator is shown in Figure 6. For the layout of the actuator the following data were used:

Amplitudes of harmonic gearbox motions at a frequency of

4Ω	= 28 Hz	:	0.03 ÷ 0.40 mm
8Ω	= 56 Hz	:	< 0.04 mm

Actuator forces

max. static force	:	20.5 kN
max. dynamic force	:	± 3.0 kN

The actuator must be able to block locally the load path to the fuselage for blade passage harmonic disturbances and to transfer at the same time static or quasi-static forces. In order to fulfil this task, static friction of the actuator must be as low as possible. This could be achieved by hydrostatic bearings, but - with respect to the helicopter - weight, length and required power could not be accepted. Thus, a commercial type actuator with balanced piston areas and specially adapted bearing seals (labyrinth seals) was chosen. The test actuator was produced by Haenchen, Stuttgart. The test results (see Figure 7 right) demonstrate the low friction characteristics. According to this diagram, maximal static friction is less than 150 N (0.7% of max. force) at a pressure of about 206 bar and an oil temperature of 25°C. For higher temperatures the value is reduced to about 100 N.

Another interesting item was the selection of the servovalve. For active isolation the controlled output variable of the actuator has to be a force or - equivalent - a pressure. Pressure control of servoactuators may be realized by pressure control servovalves or by

flow control servovalves with electric pressure feedback (see for instance Reference 5). Because of the better performances (hysteresis, linearity etc.) of flow control valves a 4-port Moog servovalve, type 30, series 31, was used for the tests in combination with a special analogue pressure feedback compensator. Moreover a by-pass throttle was integrated into the actuator in order to facilitate the control purpose by reducing the high pressure gain of flow control servovalves. The left diagram of Figure 7 illustrates that pressure gain can be varied by the by-pass throttle between

700 bar / mA (throttle closed)
and 130 bar / mA (throttle open) .

4. Theoretical Investigations

4.1 System Concept and Mathematical Description

The active isolation system uses a feedback controller based on the disturbance rejection theory (see Reference 6). Oscillatory loads can be compensated by "Notch Isolators", which are tuned to the given deterministic disturbance frequencies (4Ω = 28 Hz and 8Ω = 56 Hz). Quasi-static movements of the fuselage relative to the rotor/transmission unit can be cancelled by an integral trim compensator. Both of these tasks are fulfilled by a digital control unit, which has been chosen because of

- the complexity of the control laws of future coupled multi-axis isolation systems,
- the higher flexibility during design changes, and
- the favourable cost development in comparison with analogue devices. In addition, the realization of the digital controller enabled valuable experience to be gained in the application of digital techniques to relatively high frequency systems.

The theoretical layout of the active isolation system is based on the following concept:

- mathematical description of the complete system with actuator and servovalve dynamics (5 state variables) using an analogue PD_2 pressure feedback,
- separation of the eigenvalues of the complete system into fast and slow modes by appropriate pressure feedback coefficients,
- reduction of the system (2 state variables) by neglecting the servoactuator dynamics,
- modification of the reduced system from control input i (servovalve current) to F_I (isolator force),
- implementation of integrator and notch equations into the modified reduced system ("design model") (7 state variables),
- feedback design for the control input F_I by the Linear Optimal Control Theory and the Second Method of Liapunov (Energy Controller) in order to obtain feedback coefficients independent from hydraulic values,
- digitalization of the complete system and of the integrator

and notch equations by z-transform with various holds,

- construction of a digital control algorithm using the coefficients of the feedback transfer functions, and
- test of the dynamics of the closed-loop system with digital controllers and continuous-time designed feedback coefficients in the time and frequency domain.

This concept can be used for a single-axis system with rigid structures as well as for a multi-axis system with flexible structures.

This paper only deals with a rigid single-axis system which is shown in Figure 8. The digital controller - described in 4.3 - produces a control signal u. It is transformed into the actuator force F_A which, together with the forces of the parallel spring-damper element carrying the static load 1 g, yields the isolator force F_I. This force has to become zero, if the 4Ω and 8Ω excitation forces F_R of the rotor/transmission mass m_R shall not come through to the fuselage mass m_F.

The mathematical description of the electrohydraulic servoactuator can be seen in the block diagram in Figure 9 with the servovalve current i_{SV}, the servovalve spool stroke ε, the hydraulic flow q, the differential pressure Δp, the dynamic values of the servovalve ξ_{SV} and ω_{SV}, the gain coefficients K_i, K_ε, K_p, the actuator area A, the oil compressibility k_{oil}, and the leakage flow coefficient C_L. The dynamic behaviour of this hydraulic device can be widely varied by an analogue feedback of the differential pressure Δp and its second derivative $\Delta\ddot{p}$ which has been evaluated as an suitable configuration. Thus, the servovalve input is a linear combination of an analogue (inner loop) and a digital (outer loop) feedback signal, which control the fast (hydraulic) modes and the relatively slow (disturbance) modes, respectively:

$$i_{SV} = i_{analogue} + i_{digital}$$

$$= k_{\Delta p}\,(1 + T^2 \cdot s^2) \cdot \Delta p + \sum_j k_j \cdot x_j \quad ,$$

where k_j are the control coefficients for the state variables x_j. By means of the analogue Δp-feedback, the eigenvalues can be separated into fast and slow modes (see Figure 10), which are slow enough for digital control with a sample time (= calculation time) of 2 ms (Shannon-Theorem). Approximately the same slow eigenvalues can also be obtained in the reduced system, which neglects the servoactuator dynamics (see Table 2). Table 1 shows the general structure of the complete non-dimensional system ("Simulation Model") with the 5 state variables

$\Delta\bar{z}$, $\Delta\bar{z}'$ - actuator stroke and velocity,

$\bar{\varepsilon}$, $\bar{\varepsilon}'$ - servovalve spool stroke and velocity.

$\Delta\bar{p}$ - differential pressure,

the input variable

$\bar{i}$ - servovalve current,

the disturbance

$\bar{F}_R$ - rotor force,

and the output variables

$\bar{F}_I$ - isolator force,

$\bar{z}_F$" - fuselage acceleration,

as well as the reduced system ("Design Model") which only requires the 2 state variables

$\Delta\bar{z}$, $\Delta\bar{z}'$ - actuator stroke and velocity.

A detailed explanation of the matrix coefficients, which is beyond the topic of this paper, is given in Reference 3. - The neglection of the servoactuator dynamics results in a direct connection between input $\bar{i}$ and output $\Delta\bar{p}$ without time delay (instantaneous step response), which is physically unrealizable. Nevertheless, a controller designed for this reduced system, with a measurable state vector, can stabilize the complete system, with a partially unmeasurable state vector (servovalve stroke and velocity $\bar{\varepsilon}$ and $\bar{\varepsilon}'$).

4.2 Feedback design

In order to obtain a "standard set" of control coefficients, it is useful to modify this reduced system in such a way that the input variable is not the servovalve current i but the isolator force F_I. Hence, the plant matrix remains invariant during changes of the hydraulic system, since in this case only the input F_I depends on hydraulic values. It is easier, therefore, to modify the control coefficients by a transformation equation from input F_I to input i, than by a complete new layout of the control coefficients.

The actual feedback design was performed with the (non-dimensional) state vector

$$\underline{\bar{x}} = \text{col } (\Delta\bar{z},\ \Delta\bar{z}',\ \bar{n}_o,\ \bar{n}_1,\ \bar{n}_1',\ \bar{n}_2,\ \bar{n}_2') \quad \text{(see Figure 8).}$$

As shown in Reference 1, two concepts were used: the Linear Optimal Control Theory and the Second Method of Liapunov (Energy Control). The feedback was laid out in the continuous-time domain, because the sample frequency of the digital controller (500 Hz) is fast in comparison to the highest disturbance frequency (8Ω = 56 Hz). An example for a feedback vector designed by Optimal Control and transformed for control input $\bar{i}$ is

$$\underline{\bar{k}} = \text{col } (0.590,\ 0.167,\ -0.034,\ 1.354,\ 1.042,\ 7.176,\ 0.585).$$

It was used - without 8Ω-notch feedback - in the 4Ω-isolation tests of which the results are discussed in Section 5.2. In a combination of both feedback design methods and of simulation and hardware tests the following control vector was obtained:

$$\underline{\bar{k}} = \text{col } (0.592,\ 0.165,\ 0,\ 0.696,\ 0.761,\ 0.070,\ 0.076).$$

After first successful tests with the Optimal Control feedback, the trim integrator was not used, because the main task of the laboratory research model investigations was the isolation of oscillatory loads.

4.3 Plant and Feedback Digitalization

For frequency domain calculations and for the design of a digital control algorithm, the plant and the feedback equations had to be transformed into the z-plane. The use of a simple zero-order hold in the control variable input was not suitable, because of the fast oscillations generated by the sample-and-hold effects (see Figure 11). Thus,

a "Linear Point Connector (LPC)" (see Reference 7) was implemented according to detailed investigations published in Reference 8. It interpolates between the last and last-but-one control signal (see Figure 12), so resulting in a time delay of one sample cycle T (=2 ms) instead of 0.5 T of an ordinary zero-order hold. An additional pure time delay T results from the calculation time required by the digital controller for the feedback signal. Figure 13 shows the frequency response of both of these holds including the calculation time delay. The zero-order hold and the LPC phase shift correspond to 1.5 ωT and 2 ωT, respectively. For example, at 4Ω = 28 Hz the phase lag of the zero order hold is 30° and of the LPC 40°.

The digital control algorithm uses coefficients derived from the transfer functions of Table 3 and transformed by the "Phase-Variable Canonical Forum" (see References 10 through 12). An especially simple structure is achieved by implementing a zero-order hold for the feedback signal input into the controller. This hold creates a further time delay of 0.5 T. Figure 14 demonstrates the frequency response of the 4Ω-notch transfer function $D_{1,1}(z)$, i.e. the z-transform of the Laplace transfer-function

$$G_{1,1}(s) = \frac{1}{s^2 + \omega_1{}^2} \quad , \quad \omega_1 = 4\Omega = 28 \text{ Hz} \quad ,$$

with a zero-order hold feedback signal input. The equation shows that a notch function describes an ideal undamped oscillator. The diagrams illustrate the influence of different holds in the control signal input. The total time delay of the zero-order hold in the feedback signal input (0.5 T), the calculation time (1 T), and the zero-order hold or the Linear Point Connector in the control signal input (0.5 T or 1 T) yields the phase shift shown in Figure 14. One can see the good correspondence between measurement and calculation. A more advanced hold without any time delay in the feedback signal input ("polygonal hold", see Reference 9) or even a quasi-prediction of the control signal could be achieved by a small modification of the digital control programme. Nevertheless, the simulations and the hardware tests demonstrated that even with the phase shift of about 50° for ω = 28 Hz a good isolation can be achieved. Figure 15 shows again the advantage of a "smoothed" control input signal, interpolated by a Linear Point Connector, in comparison to a step shaped signal, created by a zero-order hold, despite the phase shift of the LPC. The Optimal Control feedback coefficients, mentioned in Section 4.2, yield a good isolation of the 4Ω = 28 Hz excitation forces.

5. Test Results

The model tests for the active rotor isolation system were carried out at the DFVLR-Institut für Aeroelastik in Göttingen. A complete description and discussion of the tests is given in References 3 and 4, Table 4 contains relevant data.

5.1 Open-Loop Tests

Natural Frequencies of the Test Rig - For the measurement of special test rig frequencies the servoactuator was replaced by an equivalent mass. This configuration yielded the following values for the

- 1. nat. frequency (soft suspension): 2.9 Hz
- 2. nat. frequency (support springs): 38.0 Hz .

The 1. natural frequency shows that a good approach to the free-free vibration state could be achieved. Some other natural frequencies of 11 Hz, 17 Hz, 63 Hz, 87 Hz etc. belong to higher modes of the guidance system.

Servoactuator Tests - As mentioned above, an analogue pressure feedback was provided for the actuator making it possible to change the dynamic behaviour in a wide range, especially to separate the eigenvalues into fast and slow modes. Based on the results of theoretical investigations, the PD_2-feedback coefficients were optimized with regard to pressure response on harmonic and step servovalve input signals. Figure 16 shows the frequency response with a nonlinearity in the support spring frequency range (38 Hz) as a function of the control input amplitude. An usual value of this amplitude is 250 mV_{eff} which can be compared with theoretical results, based on an equivalent support element damping ratio of 15% (dashed line). The numerous peaks beyond 60 Hz mainly result from higher modes of the guidance system, while the highest peak represents the actuator mode.

5.2 Closed-Loop Tests with Digital Disturbance Rejection

The first closed-loop tests for the active rotor isolation were carried out with the Optimal Control feedback.

Trim Compensator Tests - The trim integrator was tested with reference signal (Δz_o) step inputs into the digital controller (see Figure 8). The transient response of the system showed that the integrator enabled a quick trimming of the rotor/transmission-fuselage displacement.

4Ω-Vibration Isolation - Figure 17 demonstrates a typical transient response of the isolation system with the 4Ω-controller. The fuselage acceleration $\ddot{z}_F$ - proportional to the isolator force F_I because of the rigid fuselage mass - is shown in comparison to theoretical results. At the left side of the diagram both loops - analogue and digital - are open. The shaker force $F_R = \pm 1000$ N yields the fuselage acceleration $\ddot{z}_F \simeq \pm 0.13$ g. With both loops closed, the differential pressure Δp increases to a stationary amplitude of about 15 bar, enlarging the piston displacement Δz to ± 0.2 mm and, thus, cancelling the 4Ω-part of the isolator force by the inertia force of the rotor/transmission mass - the principle of nodal isolation. In the case of a rigid fuselage, this yields a vanishing of the fuselage acceleration $\ddot{z}_F$ which is demonstrated in the diagram second from bottom, where a low pass-filter with 40 Hz allows to judge the isolation of the $4\Omega = 28$ Hz disturbance (compare with the theoretical result): it vanishes after about 3 cycles $\hat{=}$ 0.1 s. The unfiltered signal contains high frequency - low amplitude oscillations which can be cancelled by some modifications of the analogue feedback and the servovalve. The offsets of the differential pressure and the piston displacement signals result from sensor offsets in connection with the proportional feedbacks.

An example of the good correspondence between measured and calculated results is given in Figure 18, where the most important variab-

les are compared during stationary isolation.

The same 4Ω-isolation case is illustrated as a frequency response plot in Figure 19. One of the most interesting criteria of an isolation system is the relation between the resultant isolator force F_I, causing the acceleration of the isolated fuselage mass m_F, and the disturbance rotor force F_R. With the rotor/transmission mass m_R, the static value of the transmissibility is

$$TR = \frac{|F_I(\omega)|}{|F_R(\omega)|} \rightarrow \frac{m_F}{m_R + m_F} \simeq 1 - \frac{m_R}{m_F} \simeq 1 \quad (\omega \rightarrow 0)$$

with $F_I(\omega)$ and $F_R(\omega)$ as the Fourier-transforms of F_I and F_R. Thus, a real reduction of the transmissibility means a value below this ratio. Figure 19 demonstrates the excellent 4Ω-isolation of the first controller of Section 4.2 designed by means of Linear Optimal Control theory. It guarantees a 90% vibration isolation during rotor frequency changes of about 3.5% (manoeuvres etc.). If the notch frequency is adapted to the rotor speed (see Figure 2), a vibration isolation of about 99% is achieved over the full range of rotor speeds. The comparison to the theoretical results shows a good correspondence; again, the differences mainly result from the guide springs which are not included in the theoretical system.

4Ω-and 8Ω-Vibration Isolation - An example of dual-frequency isolation is presented in Figure 20 where the force transmissibility is plotted versus linear frequency. The feedback vector, for this controller, was designed by the Energy Control method in theoretical and experimental investigations (see Section 4.2). The plot demonstrates that very good isolation of the 4Ω- and 8Ω-disturbances can be achieved by digital disturbance rejection. The dashed line represents the calculated results showing good agreement with measurement.

6. Conclusions

The main result of the model tests was the high performance of an active rotor isolation system with an electrohydraulic servoactuator. By means of modern control theory, it is possible to develop a very powerful device for simultaneous isolation of multi-frequent disturbances with an effectiveness of about 99%.

In the first theoretical and experimental investigations into the active vibration isolation system, the following results are obtained:

- The servoactuator combines good friction characteristics with a very high cutoff frequency.
- The analogue pressure feedback allows a clear separation between slow and fast system modes, which is advantageous for digital controlling and for further investigations with a flexible structure.
- The digital controller yields an impressive, simultaneous isolation of vibrations with 28 Hz and 56 Hz as well as a good trimming of manoeuvre loads.

- The experimental and the theoretical results show a very good correlation.

The main point of interest of further investigations and developments - planned in the near future - are

- optimization of the servoactuator dynamics by further modifications of the analogue feedback,
- reduction of the phase lag, caused by sample data systems, by means of control algorithms with polygonal holds and signal prediction,
- implementation of a rotor speed adaptation into the digital control algorithm for wideband isolation, and
- investigations of the isolation characteristics with a flexible fuselage simulated by an equivalent beam.

References

1) H. Strehlow, R. Mehlhose and M. Obermayer, Active Rotor Isolation with Application of Multi-Variable Feedback Control, Third European Rotorcraft and Powered Lift Aircraft Forum, Paper No. 23, 1977

2) G. Reichert and H. Strehlow, Untersuchungen zu einem aktiven Schwingungsisolationssystem, Messerschmitt-Bölkow-Blohm GmbH, Bericht UD-214-77-Ö, 1977

3) R. Mehlhose and M. Obermayer, Erarbeitung eines Konzepts für ein allgemein anwendbares aktives Schwingungsisolationssystem für Hubschrauber-Zellen einschließlich Funktionsnachweis im einachsigen Funktionsmodell, will be published by Bundesministerium für Forschung und Technologie

4) M. Degener, Experimentelle Untersuchungen eines aktiven Schwingungsisolationssystems für Hubschrauber an einem einachsigen Funktionsmodell, Deutsche Forschungs- und Versuchsanstalt für Luft- und Raumfahrt e.V., Interner Bericht IB 253-78 J 11, 1979

5) E. Göllner, Lineare regelungstechnische Analyse elektrohydraulischer Kraftregelungen, Ölhydraulik und Pneumatik 19, No. 12, 1975

6) E.J. Davison, The Output Control of Linear Time-Invariant Multivariable Systems with Unmeasurable Arbitrary Disturbances, IEEE Transactions on Automatic Control, Vol. AC-17 No. 5, 1972

7) S.A. Tretter, Introduction to Discrete-Time Signal Processing, John Wiley & Sons, New York, 1976

8) G. Schulz, Digitale Simulation eines vollaktiven Schwingungsisolationssystems für Hubschrauber, Deutsche Forschungs- und Versuchsanstalt für Luft- und Raumfahrt e.V., Interner Bericht IB 552-78/9, 1978

9) B.C. Kuo, Discrete Data Control Systems, Prentice Hall Inc., Englewood Cliffs, New Jersey, 1970

10) H. Kwakernaak and R. Sivan, Linear Optimal Control Systems, Wiley - Interscience, New York, 1972

11) J. Ackermann, Abtastregelung, Springer-Verlag, Berlin, 1972

12) R. Isermann, Digitale Regelsysteme, Springer-Verlag, Berlin, 1977

COMPLETE SYSTEM STATE	$\begin{bmatrix} \Delta\bar{z} \\ \Delta\bar{z}' \\ \bar{\varepsilon} \\ \bar{\varepsilon}' \\ \Delta\bar{p} \end{bmatrix}' = \begin{bmatrix} 0 & 1 & 0 & 0 & 0 \\ A_1 & A_2 & 0 & 0 & A_3 \\ 0 & 0 & 0 & 1 & 0 \\ A_4 & A_5 & A_6 & A_7 & A_8 \\ 0 & A_9 & A_{10} & 0 & A_{11} \end{bmatrix} \cdot \begin{bmatrix} \Delta\bar{z} \\ \Delta\bar{z}' \\ \bar{\varepsilon} \\ \bar{\varepsilon}' \\ \Delta\bar{p} \end{bmatrix} + \begin{bmatrix} 0 \\ 0 \\ 0 \\ B_1 \\ 0 \end{bmatrix} \cdot \bar{i} + \begin{bmatrix} 0 \\ W_1 \\ 0 \\ W_2 \\ 0 \end{bmatrix} \cdot \bar{F}_R$
COMPLETE SYSTEM OUTPUT	$\begin{bmatrix} \bar{F}_I \\ \bar{z}_{F''} \\ \Delta\bar{p} \\ \bar{\varepsilon} \end{bmatrix} = \begin{bmatrix} C_1 & C_2 & 0 & 0 & C_3 \\ C_4 & C_5 & 0 & 0 & C_6 \\ 0 & 0 & 0 & 0 & 1 \\ 0 & 0 & 1 & 0 & 0 \end{bmatrix} \cdot \begin{bmatrix} \Delta\bar{z} \\ \Delta\bar{z}' \\ \bar{\varepsilon} \\ \bar{\varepsilon}' \\ \Delta\bar{p} \end{bmatrix}$
REDUCED SYSTEM STATE	$\begin{bmatrix} \Delta\bar{z} \\ \Delta\bar{z}' \end{bmatrix}' = \begin{bmatrix} 0 & 1 \\ a_1 & a_2 \end{bmatrix} \cdot \begin{bmatrix} \Delta\bar{z} \\ \Delta\bar{z}' \end{bmatrix} + \begin{bmatrix} 0 \\ b_1 \end{bmatrix} \cdot \bar{i} + \begin{bmatrix} 0 \\ w_1 \end{bmatrix} \cdot \bar{F}_R$
REDUCED SYSTEM OUTPUT	$\begin{bmatrix} \bar{F}_I \\ \bar{z}_{F''} \\ \Delta\bar{p} \\ \bar{\varepsilon} \end{bmatrix} = \begin{bmatrix} c_1 & c_2 \\ c_3 & c_4 \\ 0 & c_5 \\ 0 & c_6 \end{bmatrix} \cdot \begin{bmatrix} \Delta\bar{z} \\ \Delta\bar{z}' \end{bmatrix} + \begin{bmatrix} d_1 \\ d_2 \\ d_3 \\ d_4 \end{bmatrix} \cdot \bar{i}$

Table 1 Matrix Equations of the Complete and Reduced Open-Loop System

	COMPLETE SYSTEM			REDUCED SYSTEM	
	RE σ/Ω	IM ω/Ω		RE σ/Ω	IM ω/Ω
SLOW MODES	-3.4842	0		-3.0024	0
	-6.9107	0		-9.6969	0
FAST MODES	-0.4271	41.9676	ACTUATOR		
	-0.4271	-41.9676			
	-63.5049	0			

Table 2 Normalized Eigenvalues of the Complete and Reduced Open-Loop System

	Compensator Transfer Function		Polyn. Coefficients with Zero-Order Hold
	Continuous-Time System	Discrete-Time System	
Integrator	$G_o(s) = \frac{1}{s}$	$D_o(z) = \frac{b_1 z + b_o}{z-1}$	$b_o = T$ $b_1 = 0$
Notch	$G_{1,\nu}(s) = \frac{1}{s^2+\omega_\nu^2}$	$D_{1,\nu}(z) = \frac{b_{2,\nu} z^2 + b_{1,\nu} z + b_{o,\nu}}{z^2 - 2z\cos\omega_\nu T + 1}$	$b_{o,\nu} = \frac{1}{\omega_\nu^2}(1-\cos\omega_\nu T)$ $b_{1,\nu} = \frac{1}{\omega_\nu^2}(1-\cos\omega_\nu T)$ $b_{2,\nu} = 0$
	$G_{2,\nu}(s) = \frac{s}{s^2+\omega_\nu^2}$	$D_{2,\nu}(z) = \frac{b_{2,\nu} z^2 + b_{1,\nu} z + b_{o,\nu}}{z^2 - 2z\cos\omega_\nu T + 1}$	$b_{o,\nu} = -\frac{1}{\omega_\nu}\sin\omega_\nu T$ $b_{1,\nu} = \frac{1}{\omega_\nu}\sin\omega_\nu T$ $b_{2,\nu} = 0$

Table 3 Compensator Transfer Functions

EQUIVALENT FUSELAGE MASS	m_F	650 kg
EQUIVALENT ROTOR/TRANSMISSION MASS	m_R	135 kg
SUPPORT SPRING STIFFNESS	k_Δ	$6.4 \cdot 10^6$ N/m
SUPPLY PRESSURE	Δp_s	206 bar (3000 psi)
HYDRAULIC FLOW (MAXIMUM)	q_{max}	9 l/min (9 cis)
HYDRAULIC FLOW (NORMAL)	q_n	2 l/min (2 cis)
SERVOVALVE - MAX. FLOW (LOAD PRESSURE DROP = 0)	q_{max}	26 l/min (26 cis)
- DAMPING RATIO	ζ_{SV}	0.5
- NAT. FREQUENCY	ω_{SV}	200 Hz
- FLOW PRESSURE COEFFICIENT	K_p	$6.2 \cdot 10^{-13}$ m^5/Ns
- FLOW GAIN	K_ε	0.664 m^2/s
- ELECTRIC GAIN	K_i	$6.41 \cdot 10^{-5}$ m/mA
ACTUATOR - MAX. STATIC LOAD	F_{st}	20.6 kN
- MAX. DYNAMIC LOAD	F_{dyn}	±3.0 kN
- WEIGHT (EXPER. VERSION)	m_A	15.9 kg
- STATIC FRICTION	F_{Fr}	≈ 100 N
- LEAKAGE FLOW COEFFICIENT	C_L	$1.0 \cdot 10^{-12}$ m^5/Ns
- PISTON AREA (BALANCED)	A	10 cm^2
- STROKE	δ_o	±2.5 mm
- LENGTH	l	262.5 mm
- OIL STIFFNESS	k_{oil}	$8.7 \cdot 10^8$ N/m
PRESSURE FEEDBACK COEFFICIENTS	$k_{\Delta p}$	$-3.95 \cdot 10^{-7}$mA m^2/N
	$k_{\Delta \ddot{p}} \hat{=} k_{\Delta p} \cdot T^2$	$-8.20 \cdot 10^{-14}$ mA m^2 s^2/N

Table 4 Data of the Active Isolation System

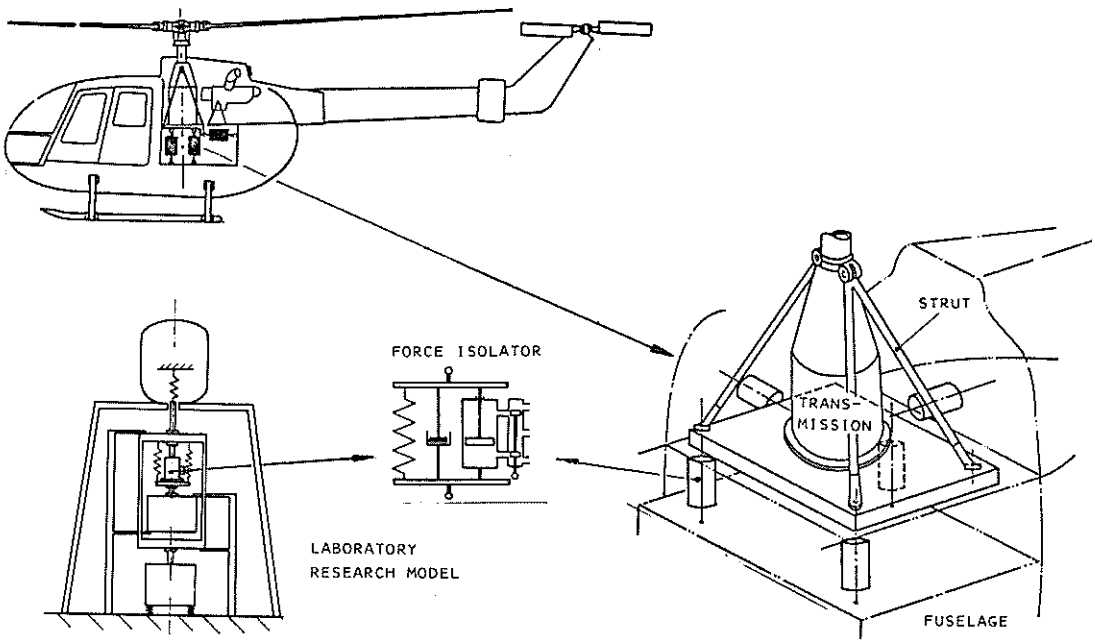

Figure 1 Concept for an Active Rotor Isolation System and Laboratory Tests

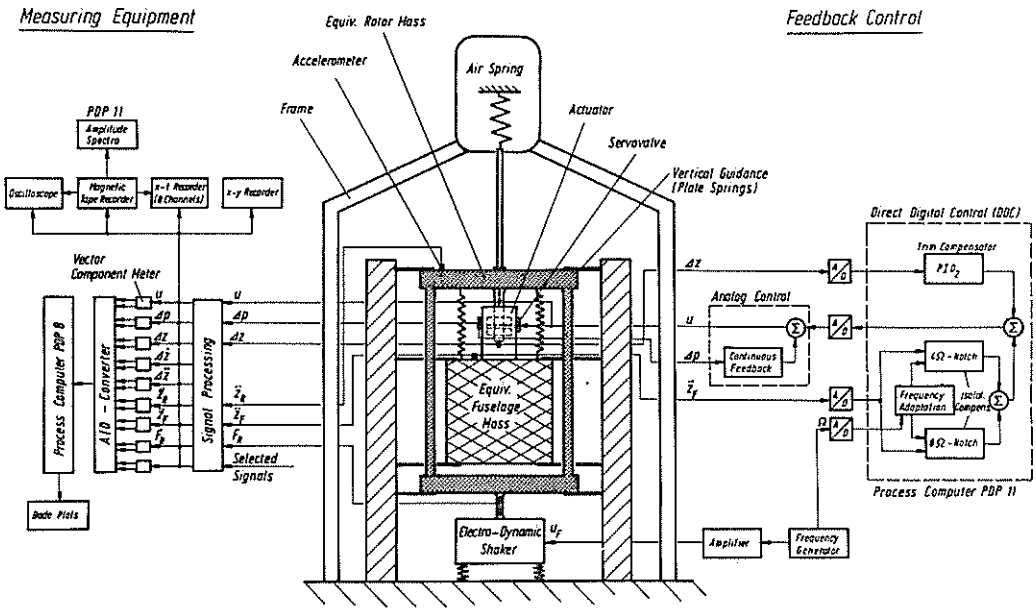

Figure 2 Laboratory Research Model

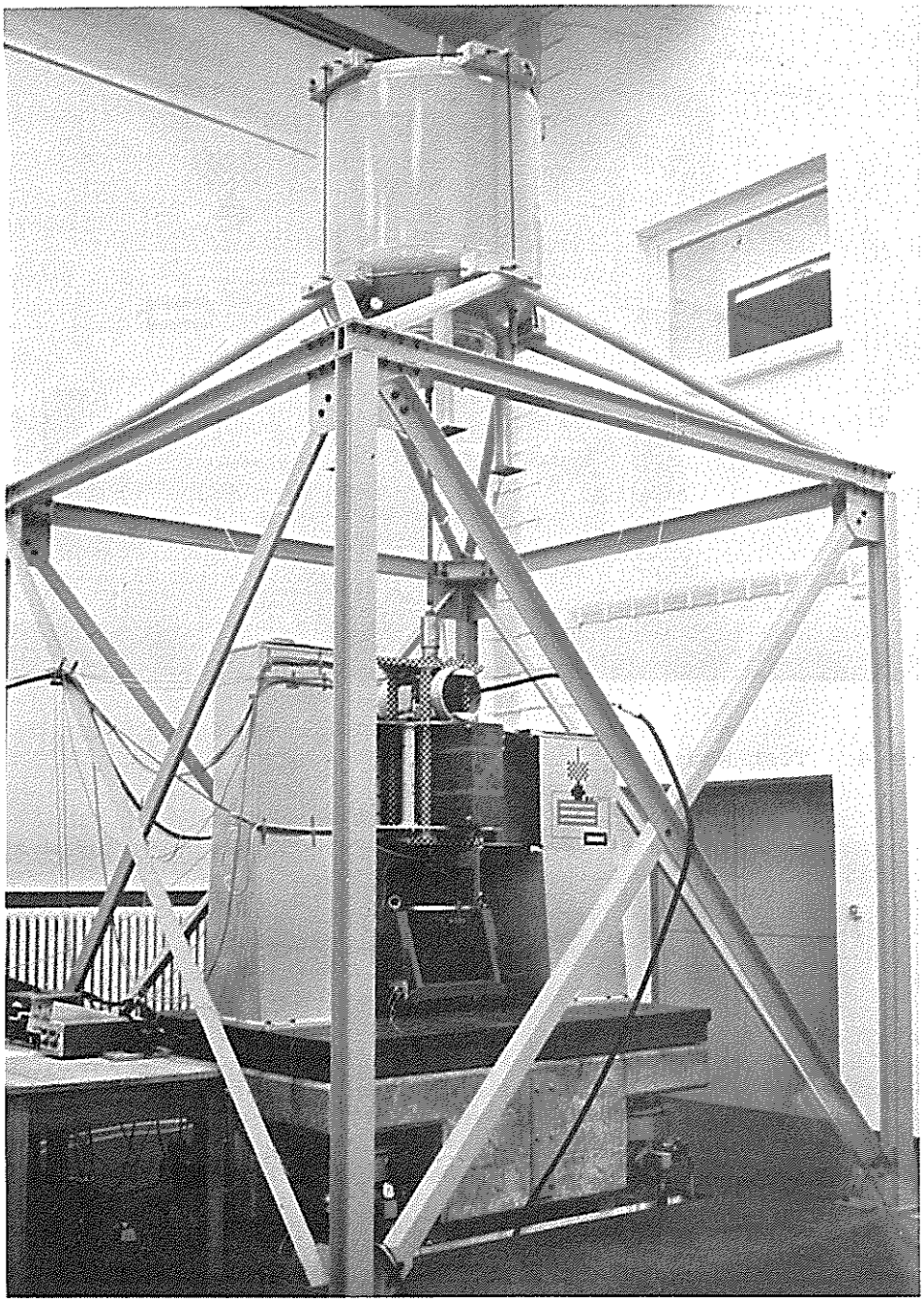

Figure 3 Test Rig

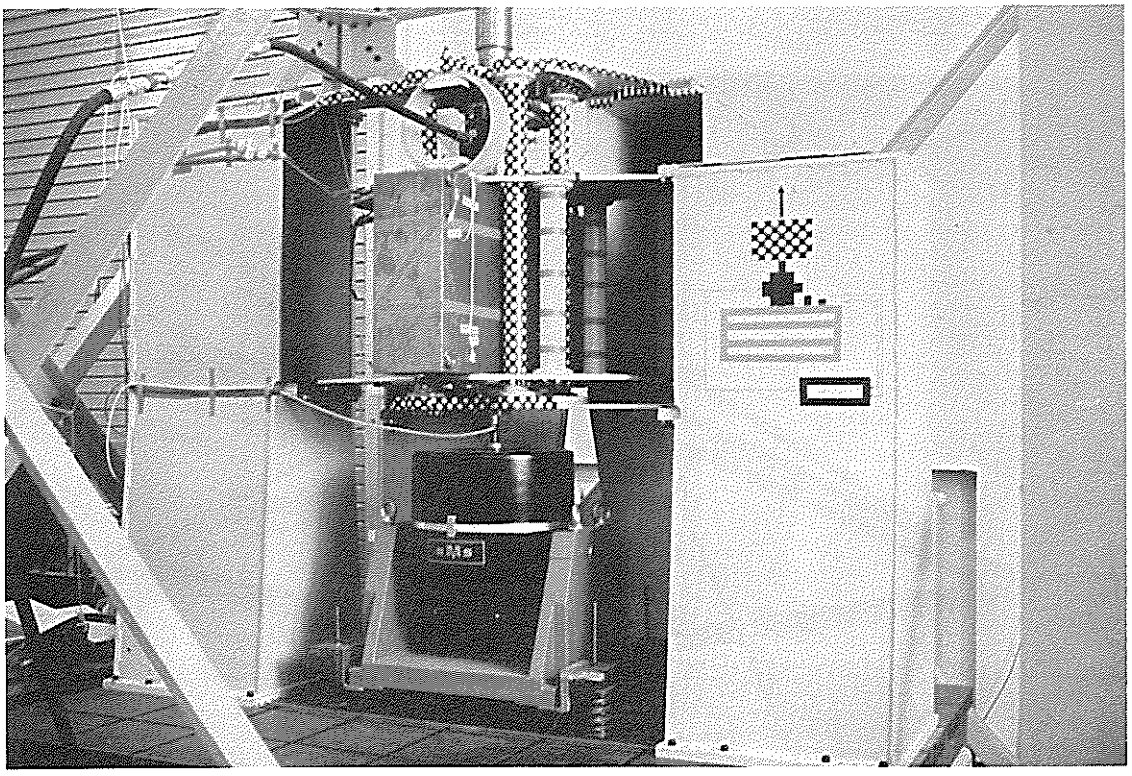

Figure 4 Test Model

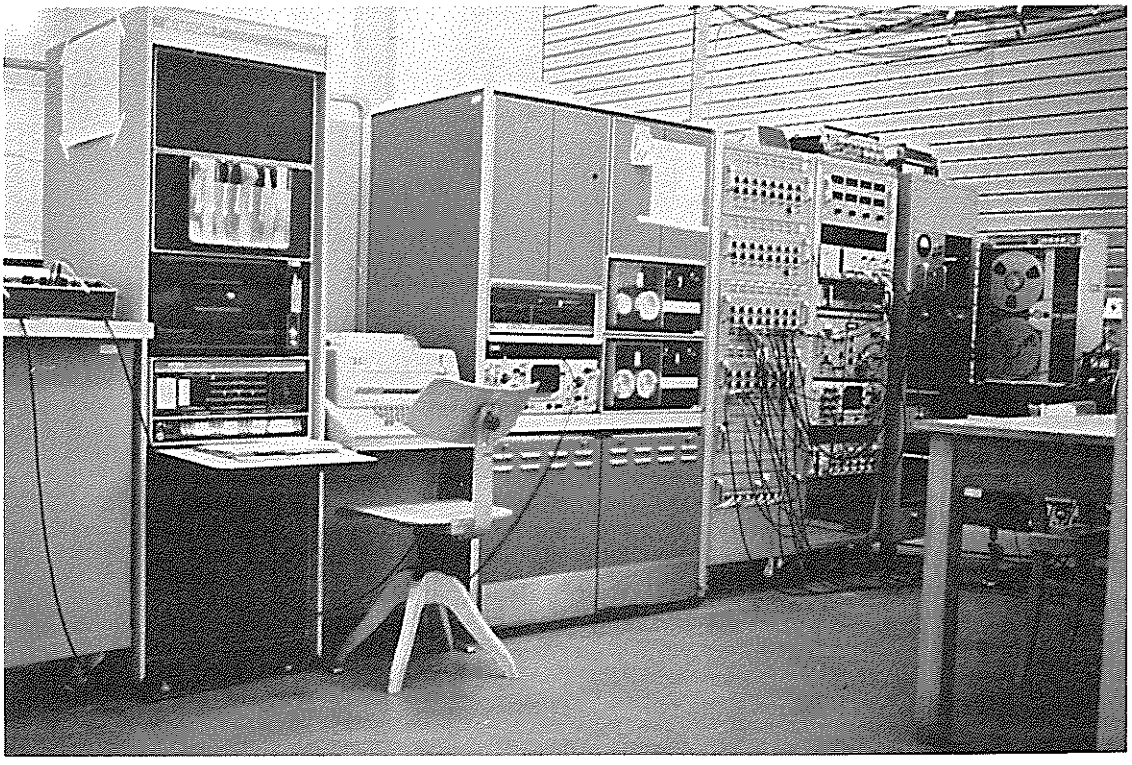

Figure 5 Measuring Equipment

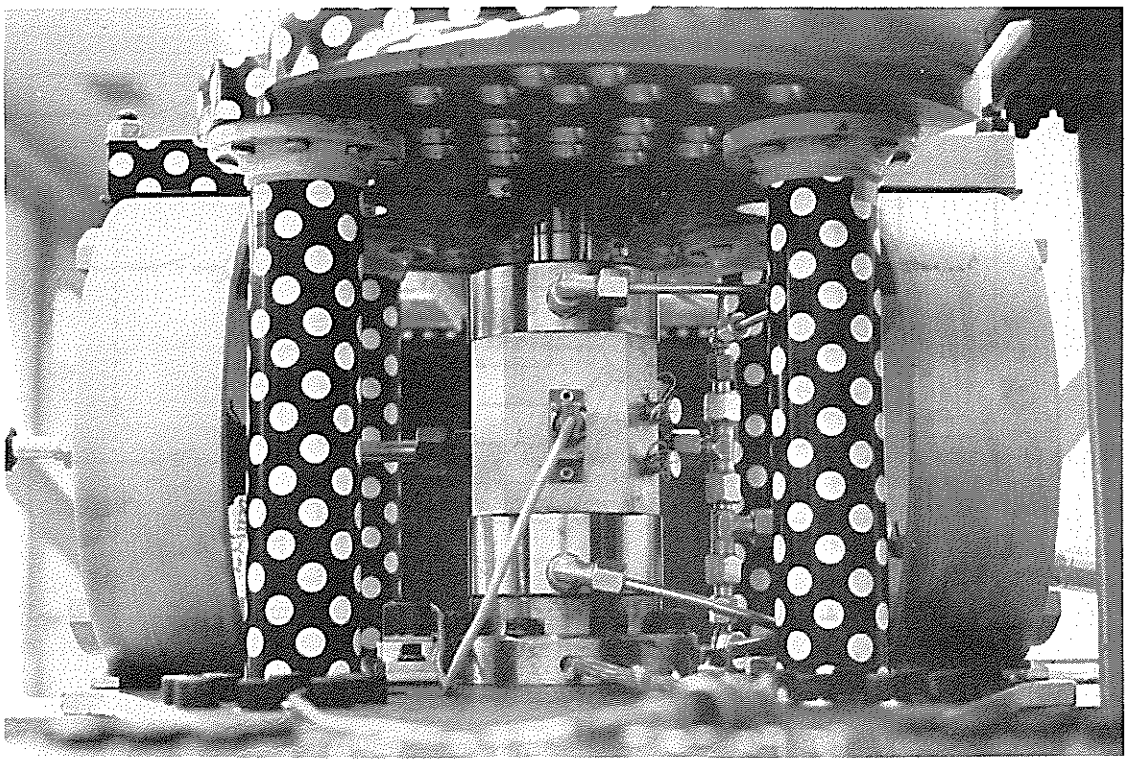

Figure 6 Servoactuator and Parallel Springs

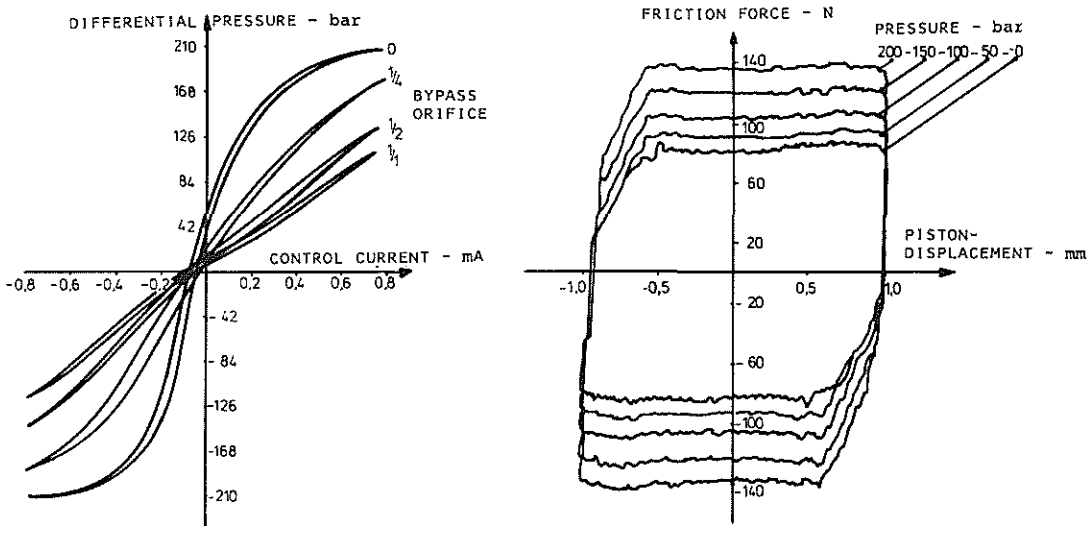

Figure 7 Static Performance of the Servoactuator

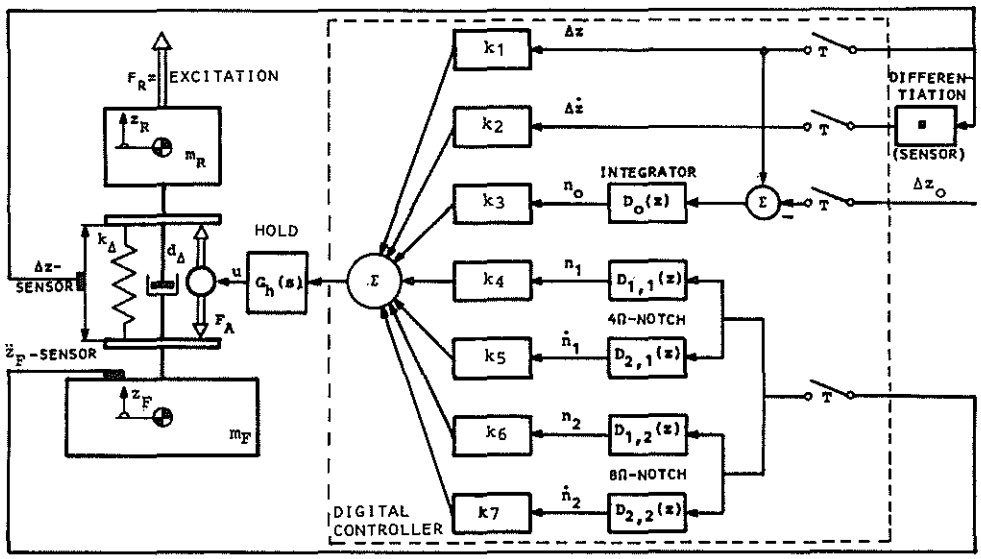

Figure 8 Single-Axis Rotor Isolation System with Digital State Feedback

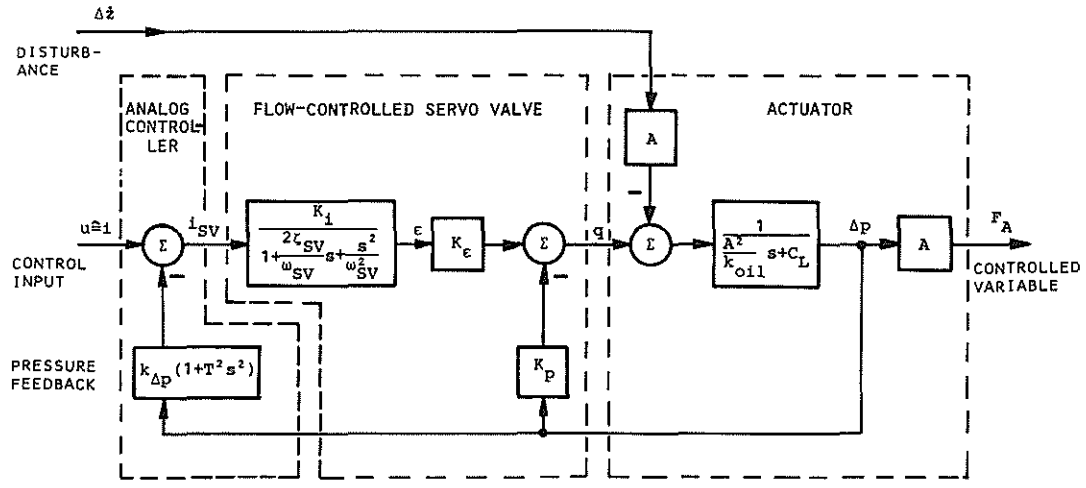

Figure 9 Block Diagram of an Servoactuator with Pressure Feedback

Figure 10

Separation of the Open-Loop Eigenvalues into Fast and Slow Modes by Pressure Feedback , and System Reduction

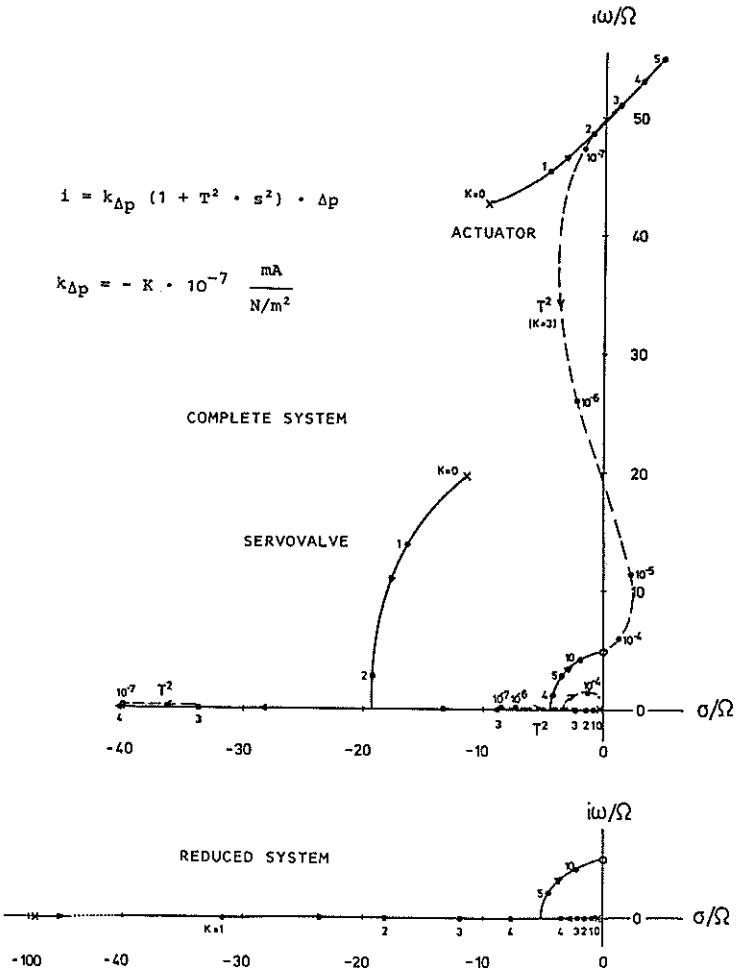

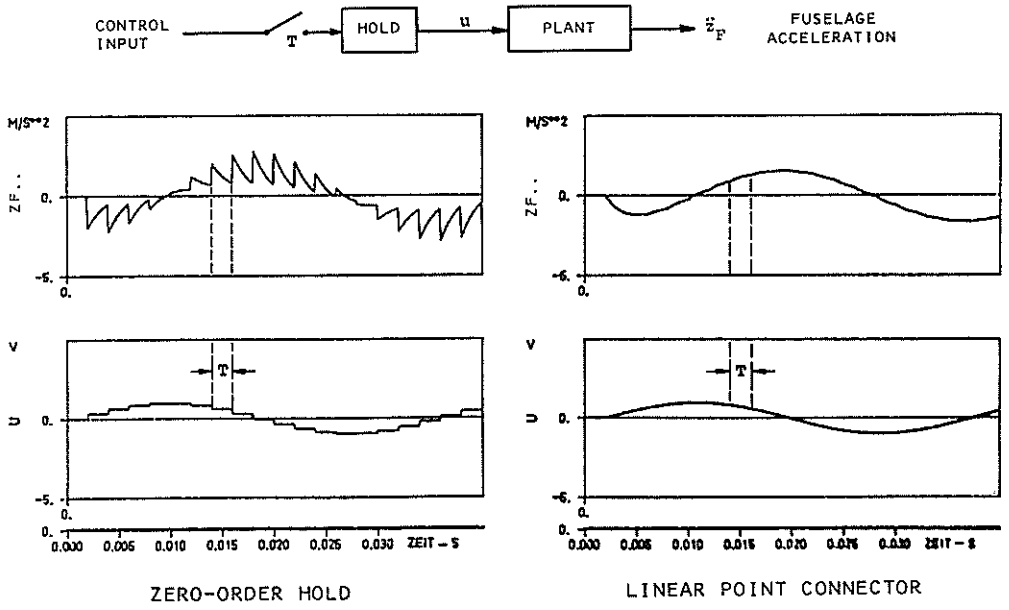

Figure 11 Sample-and-Hold Effects in Continuous-Time Systems with Sinusoidal Excitation

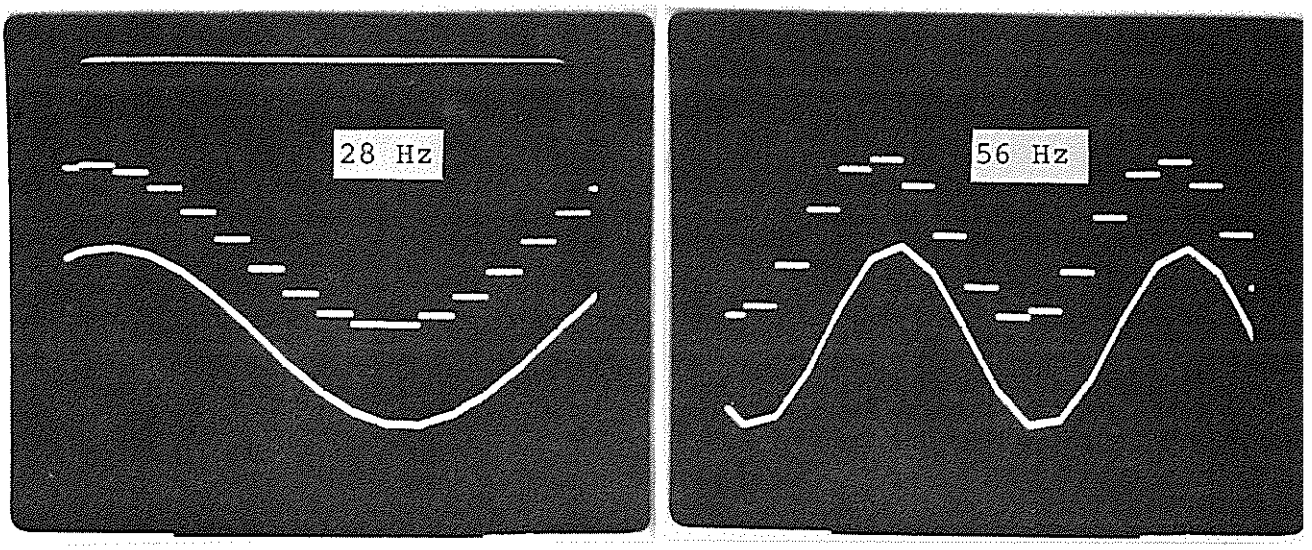

Figure 12 Zero-Order Hold and LPC Output Signals for Several Frequencies

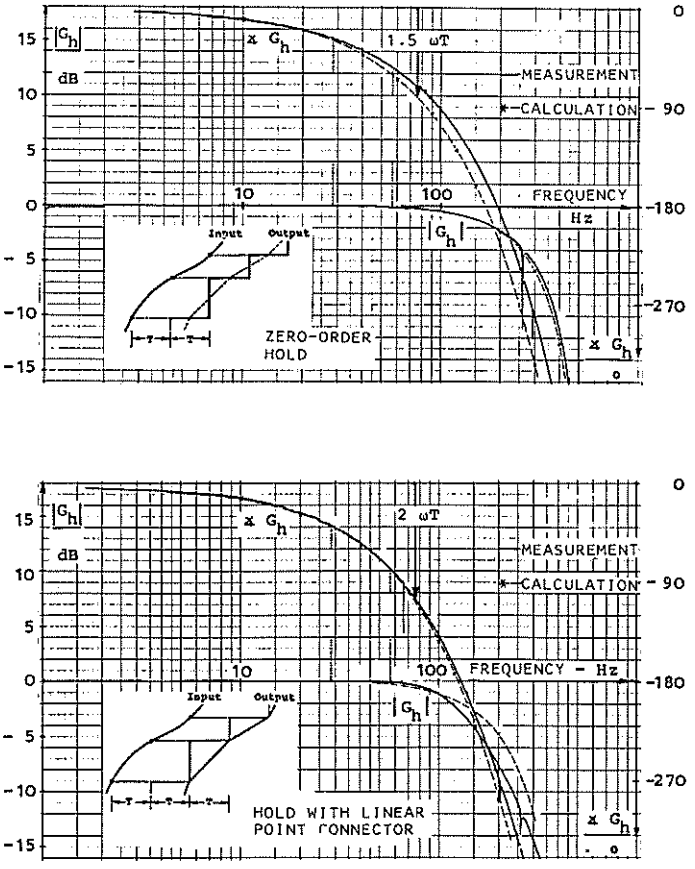

Figure 13 Frequency Response of Different Holds

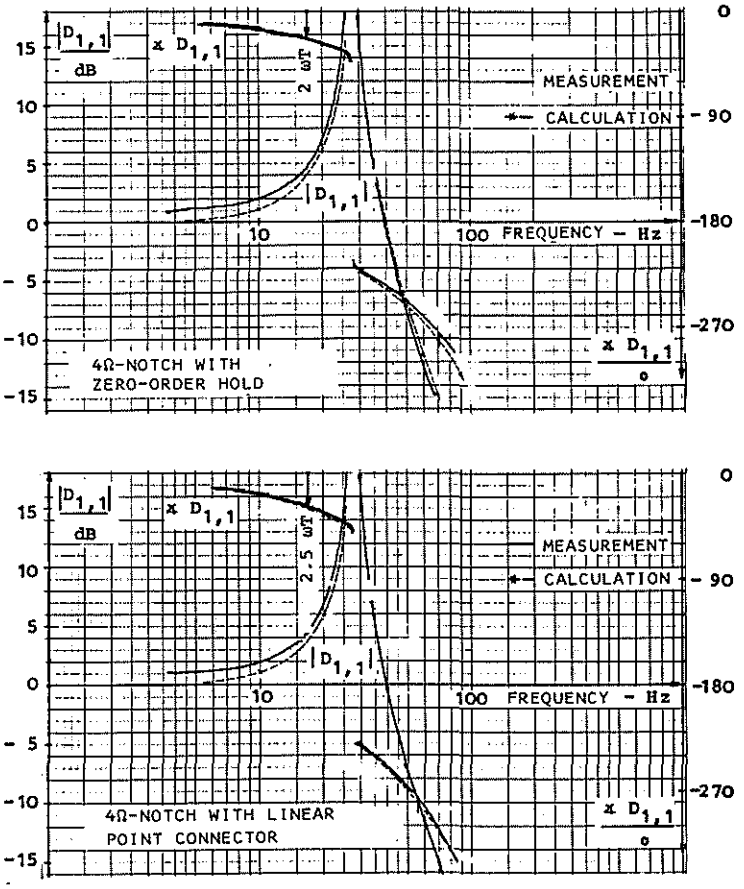

Figure 14 4Ω-Notch Frequency Response with Several Holds

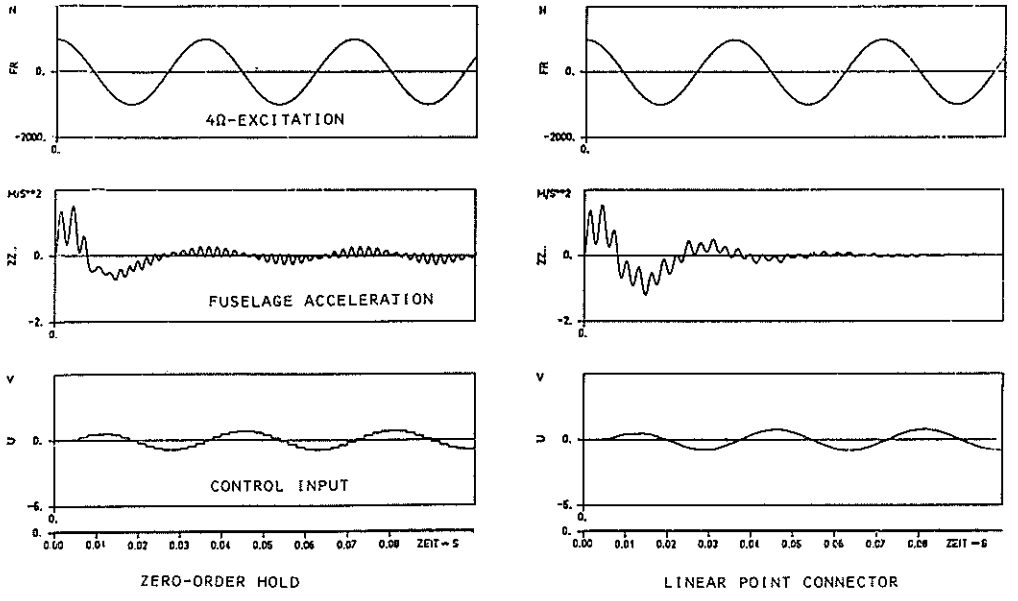

Figure 15 Sample-and-Hold Effects in an Active Vibration Isolation System (Closed Loop)

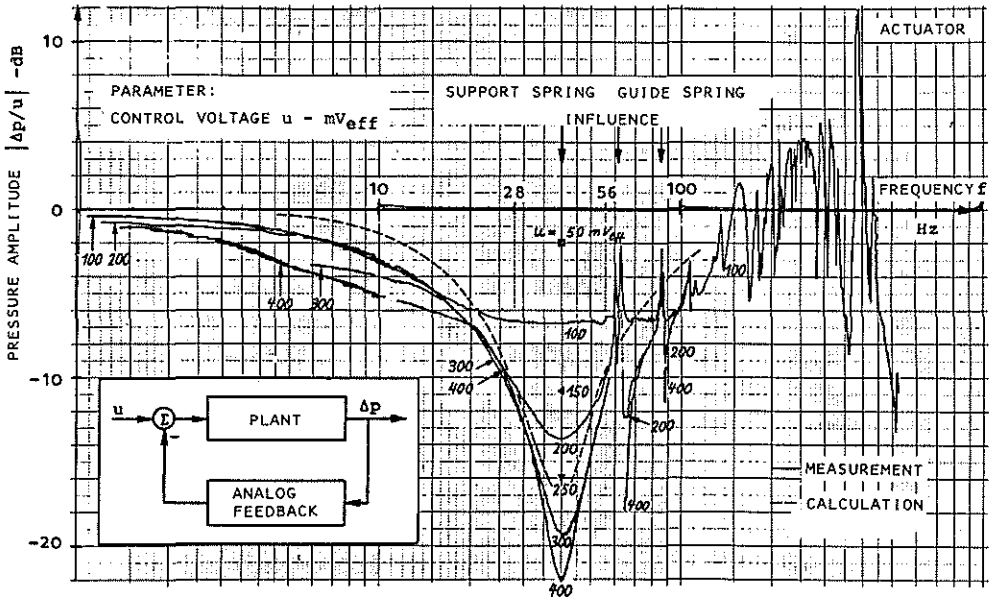

Figure 16 Pressure Frequency Response

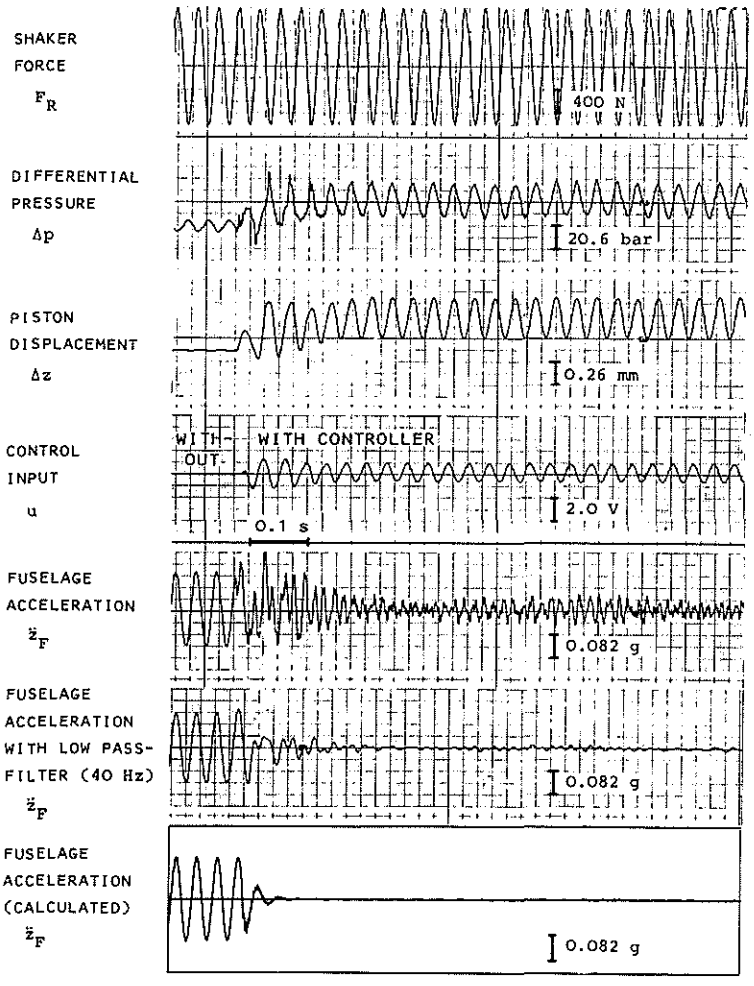

Figure 17 Transient Response of an Active Isolation System

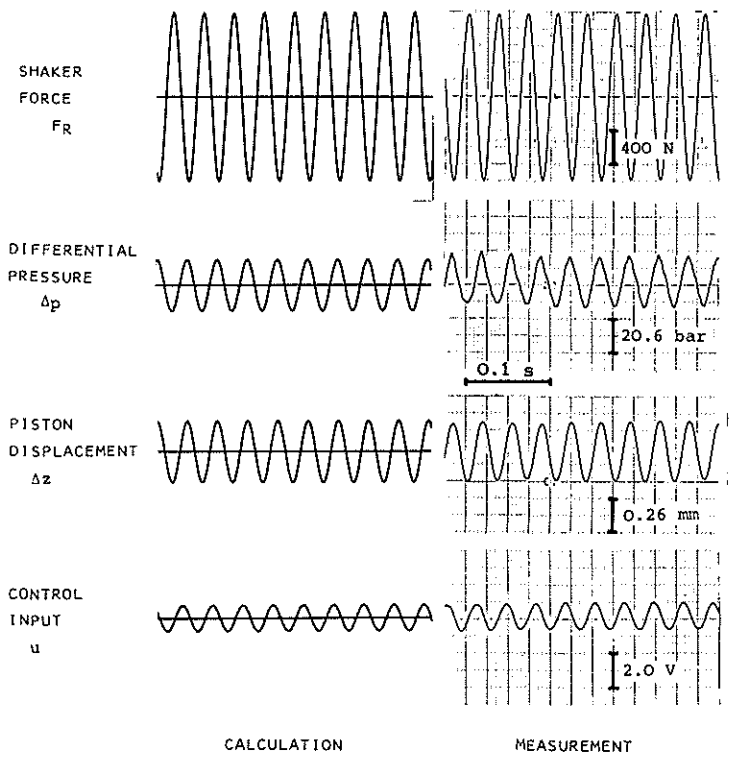

Figure 18 Comparison of Theoretical and Test Data

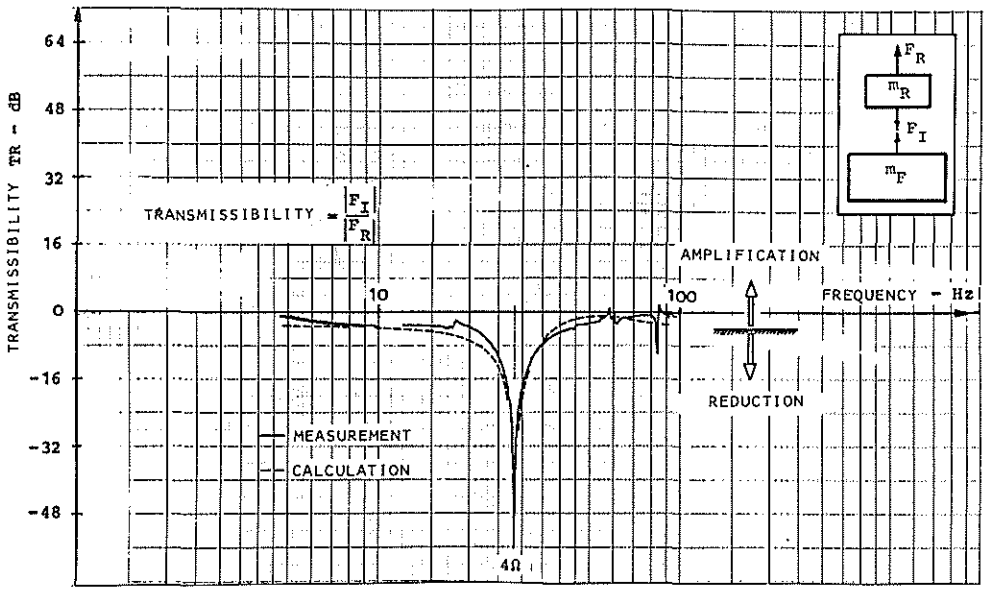

Figure 19 Force Transmissibility of a Single-Frequency Active Isolation System

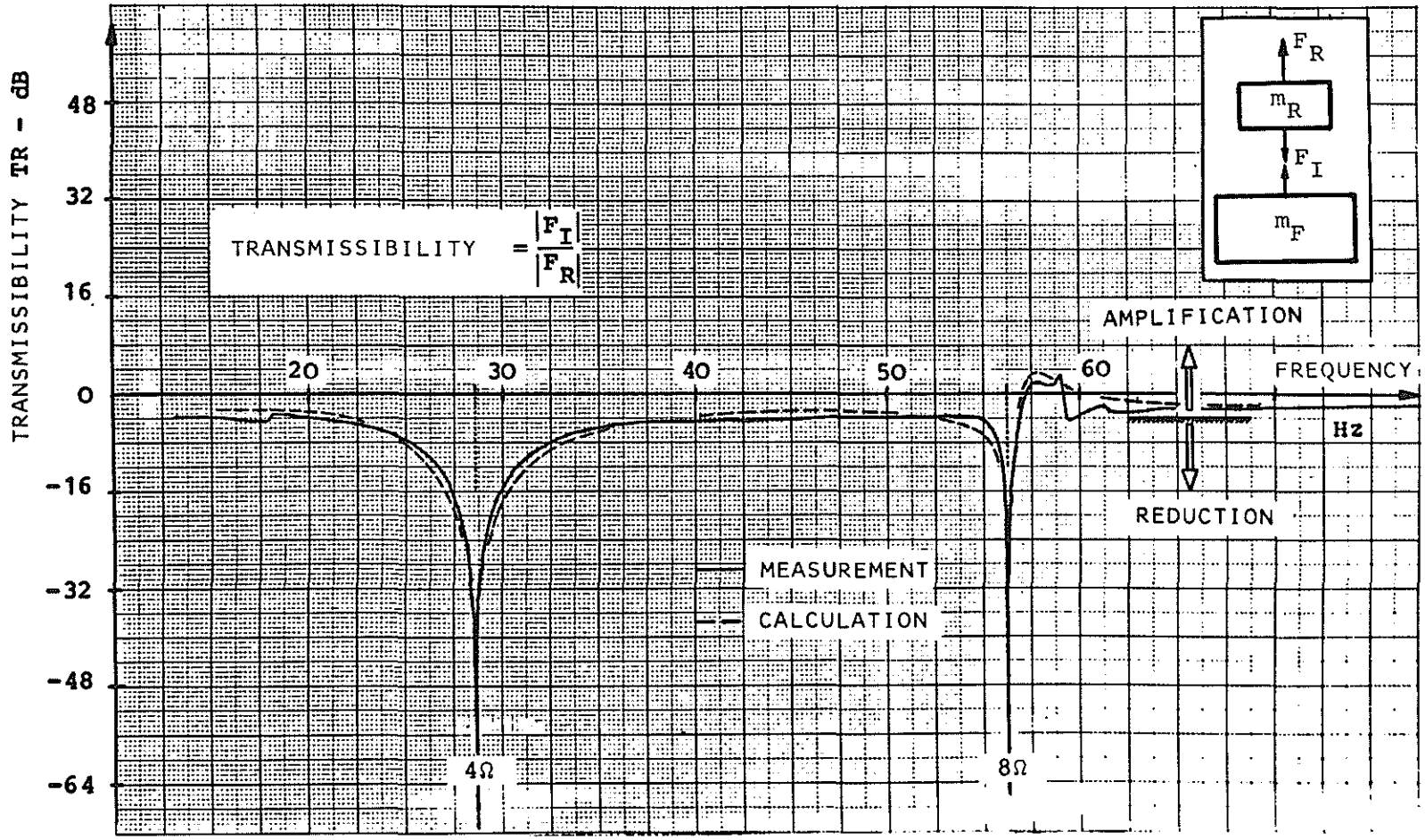

Figure 20 Force Transmissibility of a Two-Frequency Active Isolation System